Neutral photodissociation of superexcited states of molecular iodine

P. O'Keeffe
Dipartimento di Chimica, Università "La Sapienza," P. le A. Moro 5, Rome I-00185, Italy

D. Stranges
Dipartimento di Chimica, Università "La Sapienza," P. le A. Moro 5, Rome I-00185, Italy and ISMN-CNR, Sez. Roma 1, P. le A. Moro 5, Rome I-00185, Italy

P. L. Houston
Department of Chemistry, Cornell University, Ithaca, New York 14853, USA

(Received 18 May 2007; accepted 6 August 2007; published online 10 October 2007)

The formation of high-n Rydberg atoms from the neutral dissociation of superexcited states of I_2 formed by resonant two-photon excitation of molecular iodine using an ArF laser has been investigated. The high-n Rydberg atoms I^* are formed by predissociation of the optically excited molecular Rydberg states $I_2^*[R(B\ ^2\Sigma_g^+)]$ converging on the $I_2^+(B\ ^2\Sigma_g^+)$ state of the ion. Measurement of the kinetic energy release of the Rydberg I^* fragments allowed the identification of the asymptotic channels as $I^*[R(^3P_J)]+I(^2P_{3/2})$, where the $I^*[R(^3P_J)]$ are Rydberg atoms converging on the $I^+(^3P_J)$ states of the ion with $J=2$, 1, and 0. In the case of the $I^*[R(^3P_2)]$ fragments, the average Rydberg lifetime is observed to be 325 ± 25 μs. Based on experiments on the variation of the Rydberg atom signal with the field ionizing strength, the distribution of Rydberg levels peaks at about 25–50 cm^{-1} below the ionization limit. © *2007 American Institute of Physics*. [DOI: 10.1063/1.2777160]

I. INTRODUCTION

The photoionization quantum yield of a molecule excited above its ionization threshold is less than unity for many molecules.[1] This effect is due to the competition between ionization (direct or autoionization) and neutral dissociation of superexcited states (SESs), where a SES is defined as a neutral excited state with internal energy greater than the lowest ionization threshold of the molecule. These states have been the subject of a number of recent reviews in which their mechanisms of formation as well as their spectroscopy and dynamics were discussed.[2,3] In the case of a diatomic molecule, the above processes can be summarized as follows:

$$AB + h\nu \rightarrow AB^+ + e^- \tag{1a}$$

$$\rightarrow AB^{**} \rightarrow AB^+ + e^- \tag{1b}$$

$$\rightarrow AB^{**} \rightarrow A^* + B, \tag{1c}$$

where reaction (1a) illustrates direct ionization, while reactions (1b) and (1c) show the autoionization and neutral dissociation of a SES, respectively. It has been generally accepted that the SESs leading to the products in reaction (1c) are high-n molecular Rydberg states converging on each ion state, although non-Rydberg SESs have also been observed.[3] High-n Rydberg fragments from neutral dissociation of SESs have been directly observed in a small number of experiments;[4–9] however, the translational energy and angular distributions of these fragments were not measured. Extracting these data yields information on the dissociative ionic potential energy curves (PECs) as the PECs of the high-n Rydberg molecules are parallel to the ionic PECs to which they converge. Spectroscopic data on dissociative ionic curves are difficult to obtain using other techniques and therefore, this type of experiment could provide the basis for a new type of spectroscopy.

The principal photodissociation mechanism for these high-n molecular Rydberg states proposed by Freund[10] is described by the core-ion model, in which the Rydberg molecule is considered to consist of an ion core and a weakly interacting Rydberg electron. In this model the ion core dissociates, while the Rydberg electron acts as a spectator, and is then captured by a Rydberg orbital of one of the fragments at a considerable internuclear distance. Such a mechanism predicts that n should be conserved between the initially excited molecular Rydberg state and the Rydberg atom formed.

A number of combinations of excitation/detection techniques have been used to study these processes. In the 1970s one of the few sufficiently energetic sources capable of exciting such states was electron impact (see, e.g., Refs. 4 and 5). Detection methods used for high-n Rydberg fragments in combination with electron impact excitation include (i) ionization in a strong electric field, (ii) resonance ionization near a metal surface, and (iii) ionization by collision with a high electron affinity molecule. These methods allowed the extraction of the translational energy of the fragments and thus information on the potential energy curves of the excited states.

However, in more recent years the most common excitation schemes have involved photonic sources (synchrotron or laser radiation) due to the improved energy resolution of these sources. For example, based on earlier work,[11–13] Hikosaka *et al.*[8] observed fluorescing and metastable oxygen atoms following excitation of O_2 near 22 eV using synchrotron radiation. The yield curves of excited neutral particles exhibited peaks at Rydberg states converging to the ionic

core states $O_2^+(B\,^2\Sigma_g^-)$ and $O_2^+(c\,^4\Sigma_u^-)$, and the yields were strongly enhanced for high values of n. These authors subsequently employed the same technique to observe metastable Rydberg fragments from the neutral dissociation of N_2, NO, and CO.[9] Loock *et al.*[14] detected Rydberg states of I atoms in the range of $n=6-8$ from the dissociation of HI at 13.39 and 15.59 eV. The Rydbergs were observed due to their ionization by additional photons, and ion imaging was used to determine the kinetic energy release. On the other hand, Hirosaka and Mitsuke[15] employed two-dimensional photoelectron spectroscopy on this molecule in the excitation region from 11.1 to 14.85 eV, in which they observed autoionization of I atom Rydberg states converging on the excited states of the atomic ion. Using this technique, these authors also observed autoionization of atomic sulfur Rydberg states from the dissociation of carbonyl sulfide.[16] Regan *et al.*[17] observed $H(n=2)+I(^2P_{3/2})$ products following multiphoton excitation of HI, while Romanescu and co-workers[18,19] observed a similar process in HCl. Both Cl and H Rydbergs have been observed more recently by Chichinin *et al.*[20] Finally, using a version of MATI (Ref. 21) to discriminate between ions and Rydbergs, Pinnaduwage and Zhu have reported Rydberg formation in several systems following multiphoton excitation.[6,7]

Clearly, the detection techniques based on fluorescence or photoelectron spectroscopy provide information only on those fragments which have a significant fluorescence yield or a high autoionization probability and as a consequence are principally sensitive to low-n Rydberg fragments. In contrast, only very few studies have directly detected the high-n Rydberg fragments excited molecules using detectors based on field ionization.[6–9]

In this study we report resonant excitation of I_2 by two photons from an ArF laser (193 nm) into molecular Rydberg states converging on the $I_2^+(B\,^2\Sigma_g^+)$ ionic state (see Fig. 1). High-n Rydberg atomic fragments produced from the neutral dissociation of these states are directly detected by field ionization in a strong dc electric field far from the interaction region. The translational energy and angular distributions of the Rydberg fragments produced are measured.

II. EXPERIMENT

Our measurements have been carried out on a modified molecular beam apparatus[22] at the Department of Chemistry of the University of Rome "La Sapienza" which is equipped with a rotatable source and a fixed detector. Room-temperature iodine vapor was seeded at 0.04% in helium at a backing pressure of 760 Torr and expanded through a pulsed valve at a repetition rate of 80 Hz. The twice-skimmed supersonic beam was excited by the output of a focused Lambda Physik Compex 110 ArF laser at right angles. The laser spot size in the interaction region was 3×1 mm^2 and typical pulse intensities were of the order of 1 mJ. The metastable high-n Rydberg atoms formed by the two-photon photodissociation of the iodine molecules scatter out of the laser-molecular beam interaction region due to the kinetic energy departed to them by the dissociation process and fly 75.3 cm along the detector axis before being field ionized by the dc field of a Daly ion counter. The laboratory scattering angle could be varied by rotating the molecular beam source around the propagation axis of the laser. For the purpose of measuring the anisotropy of the photodissociation a Brewster plate polarizer was used to polarize the output of the ArF laser. This polarizer consists of ten 3 mm thick quartz plates placed at the Brewster angle with respect to the direction of propagation of the laser beam and yields >95% polarized light. The electric field vector of the polarized light could be rotated with respect to the detector axis by rotating the polarizer around the axis of propagation of the laser light. The speed distribution of the parent I_2 molecules in the beam was measured by recording the time of flight (TOF) distribution of the modulated beam in combination with an electron bombardment ionizer and quadrupole mass spectrometer. The TOF spectra of the atomic Rydberg fragments were simulated by forward convolution of a trial total kinetic energy release (TKER) distribution with the instrument response function and molecular beam conditions. The TKER distribution is then adjusted in an iterative manner until a good fit is obtained to all TOF spectra. A pair of parallel plate electrodes separated by 7 mm was placed ~20 cm from the interaction region along the detector axis and a small field was applied in order to remove ions. Higher field gradients could also be applied to gain information on the nature of the high-n Rydberg states (see below).

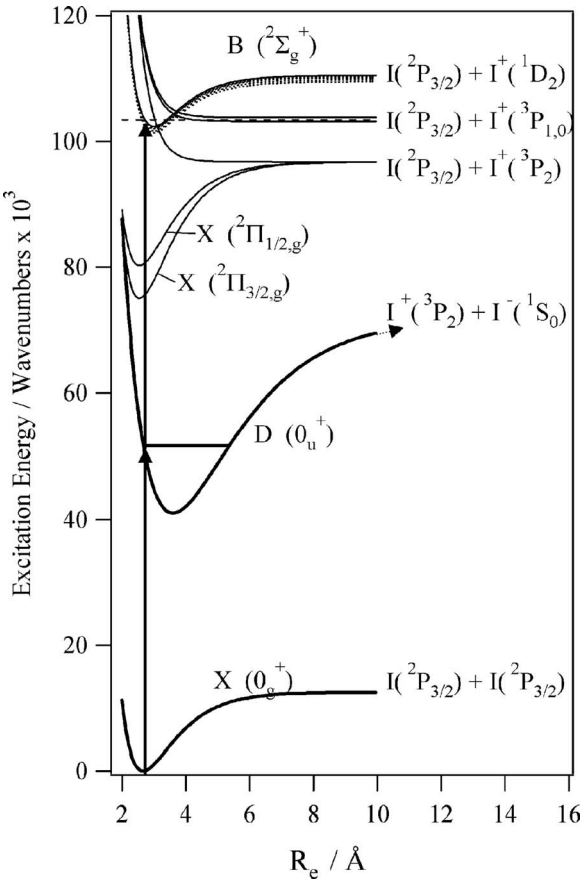

FIG. 1. Two photon excitation schemes in I_2. Thick solid lines represent the neutral potential energy curves of the I_2 while the thin solid lines show the I_2^+ potential energy curves.

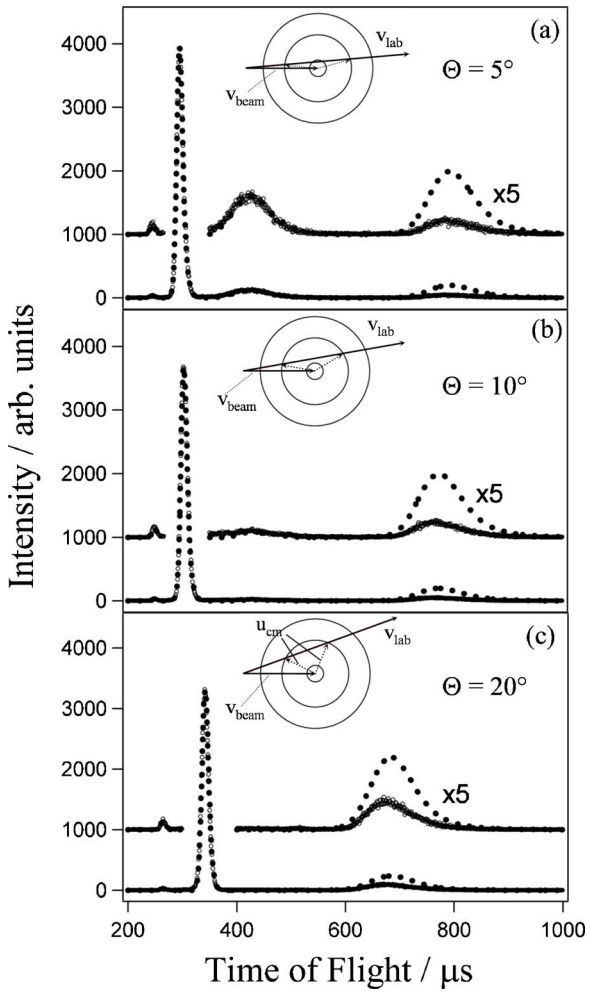

FIG. 2. Time of flight distributions and Newton diagrams of the atomic Rydberg photofragments for molecular beam to detector axis angles of (a) $\Theta=5°$, (b) $\Theta=10°$ and (c) $\Theta=20°$. The open black circles represent the experimental data while the dotted line indicates the simulations described in the text.

III. RESULTS AND DATA ANALYSIS

A. Time of flight distributions

TOF distributions of the iodine photofragment Rydberg atoms were recorded for values of the angle between the molecular beam and detector axis (Θ) equal to 3°, 4°, 5°, 7.5°, 10°, 15°, 20°, and 25°. Figure 2 shows a selection of these distributions together with their iteratively generated simulations. In the upper part of these figures the Newton circles corresponding to fragments with total TKERs of 500, 7100, and 18 900 cm^{-1} are portrayed. Also shown are the vectors representing the velocity of the beam v_{beam}, the laboratory frame vector cutting through the Newton circles v_{lab}, and the center of mass vectors corresponding to fragments with a TKER of 7100 cm^{-1} recoiling toward and away from the detector.

Examination of the TOF distributions together with the Newton circles identifies three distinct dissociation channels. First, the broad peak with maximum intensity at the arrival time of 428 μs in the $\Theta=5°$ TOF distribution is very close to the arrival time due to the beam velocity [v_{beam}(max) =1742 m/s; 433 μs] and thus is clearly due to very slowly recoiling fragments. The sharp intense peaks with arrival times of ~300 μs and the broad peaks with arrival times between 600 and 900 μs correspond to the second Newton circle where the two peaks are due to fragments recoiling toward and away from the detector, respectively. Finally, the very weak peak at early arrival times is due to the fragments corresponding to the large TKER Newton circle which recoiled toward the detector, the fragments recoiling away from the detector being too weak to be detected.

By introducing the polarizer described in the previous section into the laser beam the angle between the electric vector of the linearly polarized light and the detector axis (γ) can be varied. The TOF distributions can thus be recorded at a fixed Θ angle but as a function of the polarization angle γ. Integrating over each peak and plotting the integrated intensity against γ allow one to extract the anisotropy parameter β using the following formula:

$$I(\gamma) \propto 1 + \beta P_2(\cos(\gamma - \gamma_0)), \tag{2}$$

where γ_0 is the correction angle for the laboratory to center of mass transformation and P_2 is the second Legendre polynomial.

Using this method it has been possible to determine the β parameter for the process corresponding to the intermediate Newton circles in Fig. 2 to be $\beta=+1.00\pm0.05$ and that corresponding to the fast Newton circles to be $+0.49\pm0.03$.

Using this procedure on the slow fragments (i.e., those associated with the inner Newton circles in Fig. 2) yields a β of $+0.03\pm0.02$. However, considering that this peak contains both forward and backward scattered fragments this value of β can be considered as a lower limit of this process. In order to obtain a more accurate value of the β for this process, a further experiment was performed in which the molecular beam was directed along the detector axis, i.e., $\Theta=0$ and pinhole with diameter of 200 μm was place before the detector. Using this method the value of β can be obtained from the following formula:

$$\beta = \frac{I_{\parallel} - I_{\perp}}{(1/2)I_{\parallel} - I_{\perp}}, \tag{3}$$

where $I_{\parallel}$ is the intensity scattered parallel to the electric field vector of the excitation light and $I_{\perp}$ is that scattered perpendicular.

In this way the TOF spectra for $\gamma=0°$ and $\gamma=90°$ were recorded and the β parameter directly extracted. This procedure yielded a value of 0.14 ± 0.04 for the slow channel. The value of β determined using this method for the process corresponding to the intermediate Newton circle is $\beta=+1.03\pm0.05$, which is within the error bars of the method described above. The signal intensities for the fast process were not high enough to allow the β parameter to be measured using this method.

Combining the angular distribution data with the results of the global iterative fits of the TOF distributions (see dotted lines in Fig. 2), it has been possible to reconstruct a slice through the Newton circles (see Fig. 3) where the polarization vector of the linearly polarized light is taken to be parallel to the y axis of the plot and the intensity of the integrated signals peaked at TKERs of 0 and 18 900 cm^{-1} are

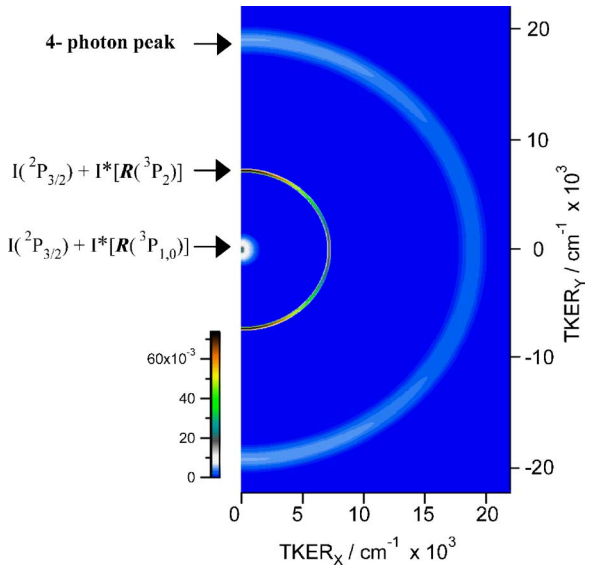

FIG. 3. (Color online) Reconstructed cuts through the Newton spheres in the center of mass using the results of the TOF simulations and angular distribution data (see text).

multiplied by 10 and 100, respectively. The processes can be assigned to the excited asymptotic dissociation limits by consulting Fig. 4.

We have assigned the circle with the TKER peaked at 0 cm^{-1} and decreasing rapidly to zero at 1500 cm^{-1} to dissociation to the $I(^2P_{3/2})+I^*[R(^3P_{1,0})]$ asymptotic limit, where $I^*[R(^3P_{1,0})]$ represents the series of Rydberg states converging on the $I^+(^3P_1)$ and $I^+(^3P_0)$ states of the atomic ion. This assignment was made after having eliminated the $I(^2P_{1/2})+I^*[R(^3P_2)]$ channel as a possible explanation for

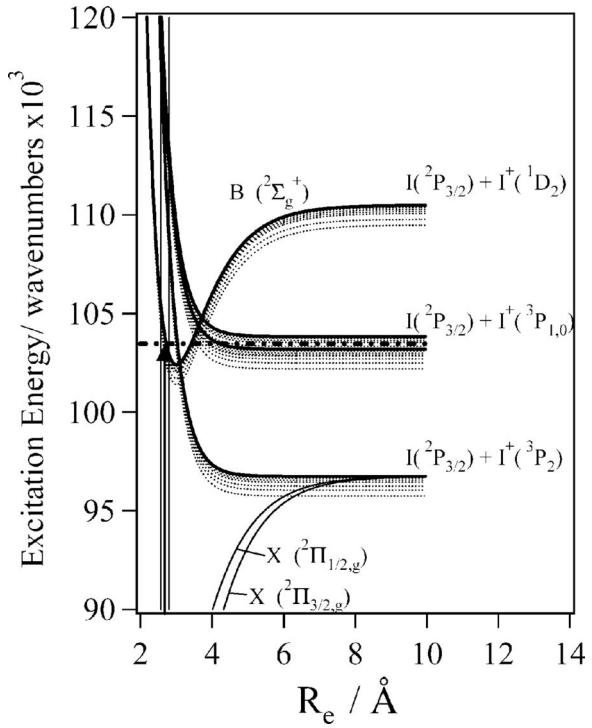

FIG. 4. Schematic potential energy curves of the ionic states together with the Rydberg states converging on each ionic state giving rise to the dissociation channels observed.

these slow fragments. The asymptotic energies of the $I(^2P_{3/2})+I^+(^3P_0)$, $I(^2P_{3/2})+I^+(^3P_1)$, and $I(^2P_{1/2})+I^+(^3P_2)$ channels with respect to the ground state of I_2 are 103 196, 103 835, and 104 351 cm^{-1}, respectively. These energies were deduced from the sum of the adiabatic ionization energy of the $I_2(X0_g^+)$ neutral ground state to the $I_2^+(X\,^2\Pi_{3/2,g})$ ionic ground state,[23] the dissociative energy of the $I_2^+(X^2\Pi_{3/2,g})$ state[23] and the spin-orbit energies of the $I^+(^3P_0)$, $I^+(^3P_1)$,[24] and $I(^2P_{1/2})$ (Ref. 25) states, respectively. Comparing these energies to the photonic energy of 103 466 cm^{-1} (two photons with wavelength of 193.3 nm) it can be seen that absorption of two photons of the peak wavelength of the ArF laser output corresponds to an energy between the $I(^2P_{3/2})+I^+(^3P_0)$ and $I(^2P_{3/2})+I^+(^3P_1)$ limits (see Fig. 4) while it is ~900 cm^{-1} below the $I(^2P_{1/2})+I^+(^3P_2)$ limit. However, the ArF laser used in this work is a broadband laser with a spectral full width at half maximum (FWHM) of ~0.5 nm and also a high energy tail which goes to zero at ~192 nm.[26] Two photons of this wavelength correspond to an energy of 104 166 cm^{-1} which is above the $I(^2P_{3/2})+I^+(^3P_1)$ limit but still almost 200 cm^{-1} below the $I(^2P_{1/2})+I^+(^3P_2)$ aysmptotic energy. This indicates that even considering only the very highest energy photons within the bandwidth of the laser (which have a correspondingly very small probability of excitation) zero fragment translational energy $I^*[R(^3P_2)]$ states formed in coincidence with $I(^2P_{1/2})$ atoms would have to correspond to Rydberg levels at least 200 cm^{-1} below the ionization potential of $I^+(^3P_2)$. This is in contradiction with the field ionization experiments described in the following section which demonstrate that 80% of the slow Rydberg fragments are ionized by a field strength of 1 kV/cm (which approximately corresponds to field ionization of Rydberg levels down to 200 cm^{-1} below the ionization threshold). In the hypothesis that the $I(^2P_{1/2})+I^*[R(^3P_2)]$ channel accounts for the slow Rydberg fragments no field ionization should occur at this field strength. It is therefore concluded that slow Rydberg fragments are principally due to high-n $I^*[R(^3P_1)]$ and $I^*[R(^3P_0)]$ Rydberg levels formed in coincidence with $I(^2P_{3/2})$ atoms and the contribution of the $I(^2P_{1/2})+I^+(^3P_2)$ channel is, if present, extremely small. The relatively wide translational energy distribution is explained by the energy splitting between the ionic states $I^+(^3P_0)$ and $I^+(^3P_1)$ and the convolution with the spectral profile of the broadband laser used to induce the two photon absorption.

The second Newton circle corresponds to a TKER distribution peaked at ~7100 cm^{-1} with a FWHM of 280 cm^{-1}. From Fig. 4 it can be seen that these Rydberg fragments are formed by dissociation to $I(^2P_{3/2})+I^*[R(^3P_2)]$, where $I^*[R(^3P_2)]$ represents the series of Rydberg states converging on the ground state of the atomic ion, i.e., the $I^+(^3P_2)$ state. Furthermore, taking into account the angular distributions and kinematics factors for these processes it was possible to deduce the branching ratio between the yields of the $I(^2P_{3/2})+I^*[R(^3P_{1,0})]$ and $I(^2P_{3/2})+I^*[R(^3P_2)]$ products to be 1:140. The final Newton circle to be assigned is that corresponding to a TKER peaked at 18 900 cm^{-1} which is greater than can be accounted for by a two-photon absorption. Power dependence studies suggest that this peak is due to a

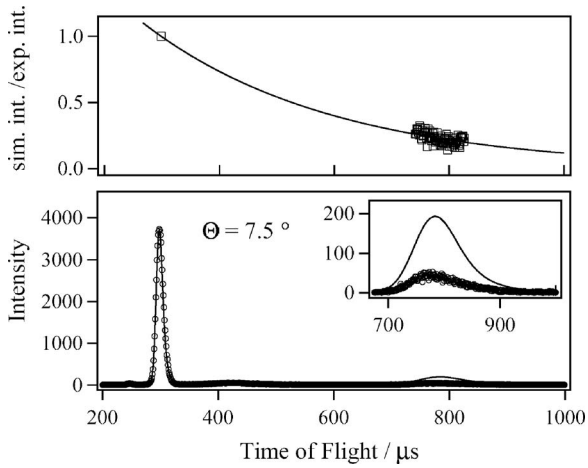

FIG. 5. Experimental TOF distribution with $\Theta=7.5°$ presented together with the simulation where an expanded view of the slower arrival times is shown in the inset of the lower panel. In the upper panel the ratio between the simulated and experimental intensities are plotted as open squares. The fit in the upper panel represents an exponential decay of the $I^*[R(^3P_2)]$ Rydberg states yielding a lifetime of $\tau=325\pm25$ μs.

four-photon absorption to one of several possible limits: $I^*[R(^1S_0)]+I[(5p^4\ ^3P_1)]6s$ (TKER of 18 900 cm^{-1}) or $I^+(^3P_2)+I^*[R(^3P_{1,0})]+e^-$ (TKERs of 18 839 and 19 478 cm^{-1}) where the energies of the Rydberg and neutral states were taken from the tabulated values of the NIST atomic spectra database.

Inspection of Fig. 2 shows that the simulated intensity for the backward scattered peak associated with the second channel is overestimated by the simulation process. Since all kinematic factors are taken into account, the explanation for this intensity difference must be due to the decay of the Rydberg atoms during their flight to the detector. It is possible to take advantage of this fact to measure the decay time of the atomic Rydberg states. The method employed is illustrated in Fig. 5. In this figure the experimental TOF distribution with $\Theta=7.5°$ is presented together with the simulation where an expanded view of the slower arrival times is shown in the inset of the lower panel. In the upper panel the ratio between the simulated and experimental intensities are plotted as open squares. As the simulation is normalized to the experimental data at the 298 μs peak, the ratio is 1.0 for this flight time. At later times the ratio decreases to values <0.25. By performing a least squares fitting procedure to these data with an exponentially decaying function it is possible to extract the lifetime for the $I^*[R(^3P_2)]$ Rydberg states. This process was repeated for the TOF distributions and simulations corresponding to $\Theta=5°$, 10°, and 20°. Examination of Fig. 2 shows that the ratio between the simulation and the experimental data increases with flight time, e.g., this ratio for the backward scattered peak in the $\Theta=5°$ distribution is ~5:1 (peak arrival time ~790 μs) while that in the $\Theta=20°$ distribution is ~2.5:1 (peak arrival time ~680 μs). This observation is consistent with the fact that the Rydberg atoms decay during their flight time to the detector. The overall result of this process yields a lifetime of $\tau=325\pm25$ μs for the $I^*[R(^3P_2)]$ Rydberg states, where the error incorporates the uncertainty in the global fits of the data corresponding to all four angles.

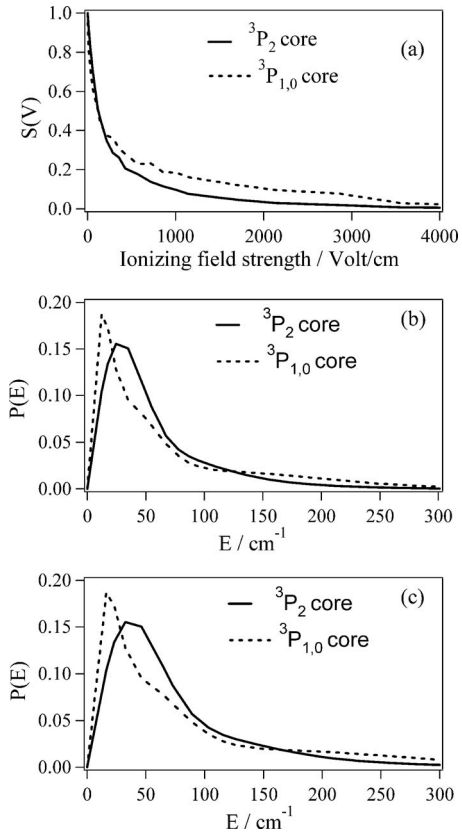

FIG. 6. The upper panel (a) shows the integrated intensity of the peaks corresponding to the forward scattered $I^*[R(^3P_2)]$ (solid line) Rydberg fragments and the scattered $I^*[R(^3P_{1,0})]$ (dotted line) Rydberg fragments plotted against the field ionization gradient. The lower two panels show the distribution of the $I^*[R(^3P_2)]$ (solid line) and $I^*[R(^3P_{1,0})]$ (dotted line) Rydberg fragment plotted against their energies below the field free ionization potential of the corresponding ions obtained by inverting the data in panel (a) (see text) using the field ionization constants of 4.6 and 6.12 for panels (b) and (c), respectively.

B. Field ionization scan

We also measured the effect of the field gradient applied between the parallel plates on the signal intensity of each peak. Instead of applying a low field gradient to eliminate ions, we varied the gradient from near 0 to more than 4 kV/cm. The resulting integrated intensities of the $\Theta=3°$ peaks at 293 μs (i.e., the $I(^2P_{3/2})+I^*[R(^3P_2)]$ channel) and at 428 μs (i.e., the $I(^2P_{3/2})+I^*[R(^3P_{1,0})]$ channels) could then be plotted against the field ionization gradient. The relationship between the ionizing field strength of a Rydberg state (V in V/cm) and the energy shift of the ionization limit from the field-free value (E in cm^{-1}) can be expressed by $E(V)=c\sqrt{V}$, where c is in the range from 4.6 to 6.12 with units of $\sqrt{\text{V cm}^{-1}}$.[27] The signal as a function of voltage, $S(V)$, decreases from 1 at zero field to 0 at an infinite field, as can be seen in Fig. 6(a), so that $1-S(V)=\int_0^{E(V)}P(E)dE$, where $P(E)$ is the population of states as a function of energy below the ionization limit. Inverting this equation yields $P(E)\propto -\sqrt{V}d(S(V))/dV$. Fitting the $S(V)$ experimental data with a triple exponential decay and performing the above conversion analytically yields the $P(E)$ distributions shown in Figs. 6(b) and 6(c) depending on whether a value of 4.6 or 6.12 is used for the field ionization constant c. For both channels the

distributions rise rapidly to maxima of 25–50 cm^{-1} below the IP and then decay slowly over a range of about 300 cm^{-1}.

IV. DISCUSSION

The dissociation of high-n molecular Rydberg states has been discussed by Freund,[10] who used a core ion model in which the high-n Rydberg electron is considered to move in a nearly hydrogenic orbital around a core consisting of a molecular ion. The nonbonding Rydberg electron interacts only very weakly with the core so that the PEC of the high-n Rydberg molecular state is parallel to that of the core ion but shifted to lower energies as determined by the quantum defect and the Rydberg formula. If the core ionic state is dissociated or predissociated by interaction with repulsive ionic states, the core dissociates following dynamics governed by the ionic PECs, while the Rydberg electron follows the ionic fragment and is captured into a Rydberg orbital of the ion at large internuclear distances. As a result n is expected to be conserved during the dissociation process.

In the case of I_2 the initial photon absorbed by the laser excites I_2 from its ground state into a range of vibrational levels ($v=142-146$) of the ion pair state D (0_u^+) (Ref. 28) which is a fully allowed one-photon transition. The second photon then promotes the molecule into a neutral state ~3.5 eV above the ionization threshold of the molecule. In this energy region of the threshold photoelectron spectrum lies a broad feature corresponding to the $B\ ^2\Sigma_g^+$ of I_2^+.[29–37] The maximum of this band is at 12.95 eV whereas the two photon energy used in this experiment corresponds to 12.83 eV with FWHM of 0.027 eV. Thus, the excited states in these experiments correspond to Rydberg states converging on the $B\ ^2\Sigma_g^+$ state of the ion.

The shapes of the PECs of the ionic states in the energy region of the $B\ ^2\Sigma_g^+$ state has been discussed by Leach[31] on the basis of results from laser photodissociation,[32] coincidence experiments on fluorescence and photodissociation[33] and photoelectron-photoion coincidence spectroscopy[34] on I_2^+, Br_2^+, and Cl_2^+, as well as calculations on the corresponding excited ionic curves. The proposed model which accounted for all of the experimental data for the entire halogen series involved the two lowest $^2\Sigma_g^+$ states. The lower of these two $^2\Sigma_g^+$ states was predicted to be extremely shallowly bound and to dissociate to the $^3P_g+{}^2P_u$ products (X^++X: spin-orbit splitting was ignored in this model), while the second $^2\Sigma_g^+$ state was proposed to be the $B\ ^2\Sigma_g^+$ state (observed in the photoelectron spectrum) and postulated to correlate with the $^1D_g+{}^2P_u$ (X^++X) products in the asymptotic region. Furthermore, in order to account for the observed $^3P_g+{}^2P_u$ products a perturbing state P was proposed to cross the B state and correlate with the ground state products. In Fig. 4 we report a modified model (in order to take into account the spin-orbit splitting) in which the $B\ ^2\Sigma_g^+$ state interacts with at least three perturbing states correlating to the three $I(^2P_{3/2})+I^*[R(^3P_J)]$ asymptotic limits. It should be noted that the lower energy $^2\Sigma_g^+$ state is not shown in this figure for clarity.

V. CONCLUSIONS

In summary, we observe the formation of high-n Rydberg iodine atoms from the neutral dissociation of the superexcited states of I_2 formed by resonant two-photon excitation. The superexcited states involved have been identified as molecular Rydberg states $I_2^*[R(B\ ^2\Sigma_g^+)]$ converging on the $I_2^+(B\ ^2\Sigma_g^+)$ state of the ion, while the measured translational energy distributions of the Rydberg fragments allowed a clear identification of the dissociation limits reached: $I^*[R(^3P_J)]+I(^2P_{3/2})$, where the $I^*[R(^3P_J)]$ are Rydberg atoms converging on the $I^+(^3P_J)$ states of the ion with $J=2$, 1, and 0. It is concluded that the initially excited molecular Rydberg state is shallowly bound but is predissociated by a number of repulsive Rydberg states correlating with the above asymptotic limits. The decay time of the atomic $I^*[R(^3P_2)]$ Rydberg states was measured to be 325 ± 25 μs. The dependence of the Rydberg fragment signal on the field ionization strength shows that the distribution of Rydberg states peaks about 25–50 cm^{-1} below the ionization limit.

The results of these experiments suggest the possibility of a new type of spectroscopy for repulsive states of ions based on simultaneous measurement in the process $AB+h\nu \rightarrow A+B(n)$ [where $B(n)$ is a Rydberg fragment with $n>20$] of (a) the frequency at which Rydbergs are produced, (b) the kinetic energy release between the fragments, and (c) the angular distribution of products. The frequency locates the electronic state leading to dissociative ionization, while the kinetic energy release identifies the final products of the dissociation. The angular distribution helps to identify the symmetry of the dissociative state. A strong advantage of this spectroscopy is that it is virtually free from background. This form of spectroscopy is sensitive to dissociative and predissociative ionic states and therefore, is complementary to the existing techniques of photoelectron, threshold photoelectron, zero kinetic energy, and mass analyzed threshold ionization spectroscopies which are principally sensitive to probing of bound ionic states. Of course, this spectroscopy requires tunable laser light, though not necessarily in the vacuum ultraviolet. For example, in a molecule such as CF_3I, recently studied by Aguirre and Pratt[38,39] and by Waits *et al.*,[40] the ionization potential of CF_3I is 10.3716 eV, and the dissociation energies for CF_3I^+ to $CF_3^+ + I(^2P_{3/2})$ or $CF_3 + I^+(^3P_2)$ are 1.012 and 2.41 eV, respectively. Thus, dissociative ionization to CF_3^+ is possible above 11.384 eV (or three photons at wavelengths below 326 nm), whereas dissociative ionization to I^+ is possible above 12.782 eV (or three photons at wavelengths below 291 nm). Much of the structure in the mass-selected ion yield curve measured by Waits *et al.*[40] near 303 nm has been assigned to resonances at the two-photon level, where there are several vibrational levels of the $[X\ ^2E_{3/2}]6p$ Rydberg state. An ideal situation would be to excite one of these with two photons of one color, and then tune a second color to detect Rydberg CF_3 or Rydberg I atoms produced from repulsive states converging to dissociative ionization curves.

ACKNOWLEDGMENTS

This research was supported by the Italian Ministero dell'Università e della Ricerca-MUR (PRIN 2005) and the

Sixth European Community Framework Programme (Contract No. MEIF-CT-2005-024895). One of the authors (P.L.H.) acknowledges support from the National Science Foundation under Grant No. CHE-0548867.

[1] J. Berkowitz, *Photoabsorption, Photoionization and Photoelectron Spectroscopy* (Academic, New York, 1979).
[2] Y. Hatano, Phys. Rep. **313**, 109 (1999).
[3] Y. Hatano, J. Electron Spectrosc. Relat. Phenom. **119**, 107 (2001).
[4] R. S. Freund, J. Chem. Phys. **54**, 3125 (1971).
[5] J. A. Schiavone, K. C. Smyth, and R. S. Freund, J. Chem. Phys. **63**, 1043 (1975).
[6] L. A. Pinnaduwage and Y. Zhu, Chem. Phys. Lett. **277**, 147 (1997).
[7] L. A. Pinnaduwage and Y. Zhu, J. Chem. Phys. **108**, 6633 (1998).
[8] Y. Hikosaka, P. Lablanquie, M. Ahmad, R. I. Hall, J. G. Lambourne, F. Penent, and J. H. D. Eland, J. Phys. B **36**, 4311 (2003).
[9] Y. Hikosaka, P. Lablanquie, M. Ahmad, F. Penent, J. H. D. Eland, and R. I. Hall, J. Phys. B **37**, 283 (2004).
[10] R. S. Freund, in *Rydberg States of Atoms and Molecules*, edited by R. F. Stebbings and F. B. Dunning (Cambridge University Press, Cambridge, 1983), Chap. 10.
[11] M. Ukai, S. Machida, M. Kitajima, N. Kouchi, Y. Hatano, and K. Ito, Phys. Rev. Lett. **74**, 239 (1995).
[12] H. Liebel, S. Lauer, F. Vollweiler, R. Muller-Albrecht, A. Ehresmann, H. Schmoranzer, G. Mentzel, and K.-H. Shartner, Phys. Lett. A **267**, 357 (2000).
[13] K. Codling, L. J. Frasinski, and K. J. Randall, J. Phys. B **18**, L251 (1985).
[14] H.-P. Loock, B. L. G. Bakker, and D. H. Parker, Can. J. Phys. **79**, 211 (2001).
[15] Y. Hikosaka and K. Mitsuke, J. Chem. Phys. **121**, 792 (2004).
[16] Y. Hikosaka, H. Hattori, and K. Mitsuke, J. Chem. Phys. **110**, 335 (1999).
[17] P. M. Regan, D. Ascenzi,. E. Wrede, P. A. Cook, M. N. R. Ashfold, and A. J. Orr-Ewing, Phys. Chem. Chem. Phys. **2**, 5364 (2000).
[18] C. Romanescu, S. Manzhos, D. Boldovsky, J. Clarke, and H.-P. Loock, J. Chem. Phys. **120**, 767 (2004).
[19] S. Manzhos, C. Romanescu, H.-P. Loock, and J. G. Underwood, J. Chem. Phys. **121**, 11802 (2004).
[20] A. I. Chichinin, C. Maul, and K.-H. Gericke, J. Chem. Phys. **124**, 224324 (2006).
[21] P. M. Johnson and L. Zhu, Int. J. Mass Spectrom. Ion Process. **131**, 193 (1994).
[22] The appartus in Rome used in these experiments is very similar to that described in D. Stranges, M. Stemmler, X. Yang, J. D. Chesko, A. G. Suits, and Y. T. Lee, J. Chem. Phys. **109**, 5372 (1998).
[23] M. C. R. Cockett, R. J. Donovan, and K. P. Lawley, J. Chem. Phys. **105**, 3347 (1996).
[24] W. C. Martin and C. H. Corliss, J. Res. Natl. Bur. Stand., Sect. A **64A**, 443 (1960).
[25] L. Minnhagen, Ark. Fys. **21**, 415 (1962).
[26] Lambda Physik Inc. (private communication).
[27] T. P. Softley, Int. Rev. Phys. Chem. **23**, 1 (2004).
[28] M. Bartels, R. J. Donovan, A. J. Holmes, P. R. R. Langridge-Smith, M. A. MacDonald, and T. Ridley, J. Chem. Phys. **91**, 7355 (1989).
[29] A. J. Yencha, M. C. R. Cockett, J. G. Goode, R. J. Donovan, A. Hopkirk, and G. C. King, Chem. Phys. Lett. **229**, 347 (1994).
[30] T. Ridley, D. A. Beattie, M. C. R. Cockett, K. P. Lawley, and R. J. Donovan, Phys. Chem. Chem. Phys. **4**, 1398 (2002).
[31] S. Leach, J. Phys. Chem. **92**, 5373 (1988).
[32] R. G. Mc Loughlin, J. F. Morrison, and D. L. Smith, Int. J. Mass Spectrom. Ion Process. **58**, 201 (1984).
[33] R. P. Tuckett, E. Castellucci, M. Bonneau, G. Dujardin, and S. Leach, Chem. Phys. **92**, 43 (1985).
[34] J. H. D. Eland, J. Chem. Phys. **70**, 2926 (1979).
[35] W. A. de Jong, L. Visscher, and W. C. Nieuwport, J. Chem. Phys. **107**, 9046 (1997).
[36] B. Niederjohann, Ph.D. thesis, University of Bielefeld, 2004.
[37] S. Unny, Y. Du, L. Zhu, R. J. Gordon, A. Sugita, M. Kawasaki, Y. Matsumi, and T. Seideman, Phys. Rev. Lett. **86**, 2245 (2001).
[38] F. Aguirre and S. T. Pratt, J. Chem. Phys. **118**, 6318 (2003).
[39] F. Aguirre and S. T. Pratt, J. Chem. Phys. **119**, 9476 (2003).
[40] L. D. Waits, R. J. Horwitz, R. G. Daniel, J. A. Guest, and J. R. Appling, J. Chem. Phys. **97**, 7263 (1992).